Electron Tomography Imaging of Surface Glycoproteins on Human Parainfluenza Virus 3: Association of Receptor Binding and Fusion Proteins before Receptor Engagement

Long Gui,[a,b] Eric M. Jurgens,[c] Jamie L. Ebner,[a] Matteo Porotto,[c] Anne Moscona,[c,d] Kelly K. Lee[a,b,e]

Department of Medicinal Chemistry, University of Washington, Seattle, Washington, USA[a]; Biological Physics Structure and Design Graduate Program, University of Washington, Seattle, Washington, USA[b]; Department of Pediatrics, Weill Medical College of Cornell University, New York, New York, USA[c]; Department of Microbiology and Immunology, Weill Medical College of Cornell University, New York, New York, USA[d]; Department of Microbiology, University of Washington, Seattle, Washington, USA[e]

ABSTRACT   In order to deliver their genetic material to host cells during infection, enveloped viruses use specialized proteins on their surfaces that bind cellular receptors and induce fusion of the viral and host membranes. In paramyxoviruses, a diverse family of single-stranded RNA (ssRNA) viruses, including several important respiratory pathogens, such as parainfluenza viruses, the attachment and fusion machinery is composed of two separate proteins: a receptor binding protein (hemagglutinin-neuraminidase [HN]) and a fusion (F) protein that interact to effect membrane fusion. Here we used negative-stain and cryo-electron tomography to image the 3-dimensional ultrastructure of human parainfluenza virus 3 (HPIV3) virions in the absence of receptor engagement. We observed that HN exists in at least two organizations. The first were arrays of tetrameric HN that lacked closely associated F proteins: in these purely HN arrays, HN adopted a "heads-down" configuration. In addition, we observed regions of complex surface density that contained HN in an apparently extended "heads-up" form, colocalized with prefusion F trimers. This colocalization with prefusion F prior to receptor engagement supports a model for fusion in which HN in its heads-up state and F may interact prior to receptor engagement without activating F, and that interaction with HN in this configuration is not sufficient to activate F. Only upon receptor engagement by HN's globular head does HN transmit its activating signal to F.

IMPORTANCE   Human parainfluenza virus 3 (HPIV3) is an enveloped, ssRNA virus that can cause serious respiratory illness, especially in children. HPIV3, like most other paramyxoviruses, uses two specialized proteins to mediate cell entry: the fusion protein (F) and the receptor binding protein, hemagglutinin-neuraminidase (HN). F becomes activated to mediate fusion during entry when it is triggered by a signal from HN. Here we used electron tomography to reconstruct the 3-dimensional ultrastructure of HPIV3. From these structures, we could discern the distribution and, in some cases, conformation of HN and F proteins, which provided an understanding of their interrelationship on virions. HN is found in arrays alone in one conformation and interspersed with prefusion F trimers in another. The data support a model of paramyxovirus membrane fusion in which HN associates with F before receptor engagement, and receptor engagement by the globular head of HN switches the HN-F interaction into one of fusion activation.

Address correspondence to Kelly K. Lee, kklee@uw.edu, Anne Moscona, Anm2047@med.cornell.edu, or Matteo Porotto, Map2028@med.cornell.edu.

The enveloped RNA viruses of the paramyxovirus family, in most cases, employ two surface glycoproteins to carry out the entry stage of the viral life cycle (1, 2). A receptor binding protein—hemagglutinin-neuraminidase (HN) for human parainfluenza virus 3 (HPIV3) or H or G, depending on the virus—binds to the viral receptor on the host cell plasma membrane, and a separate membrane fusion (F) protein, once activated by the receptor binding protein, mediates the fusion of virus and host membranes in order to deliver the viral ribonucleoprotein into the host cell. Paramyxovirus F proteins convert from a metastable prefusion form to a highly stable postfusion form when the appropriate biological trigger is sensed or in some cases when exposed to

extremes of temperature (1, 3, 4). Our observation that active participation of receptor-engaged HN is required for the F-mediated fusion process (5–7) is consistent with subsequent studies showing that the HN interaction is necessary in order to activate the fusion machinery and that engagement of the HN (or H or G) with the respective receptor is critical for fusion (1, 2, 8–13).

Current models of paramyxovirus surface glycoprotein interaction during fusion activation and viral entry posit that either (i) the HN-F interaction occurs in the absence of a receptor and "clamps" the two proteins together until the proper time, when F is released to proceed towards fusion, or (ii) the HN-F interaction

occurs only upon receptor binding, and the receptor binding protein provides the "trigger," after which F proceeds to fusion (8, 9, 14–21). For morbilliviruses, the fusion protein is stable in its prefusion configuration even without associated receptor binding protein (H); as for HPIV3 HN, H decreases the activation energy hurdle for fusion triggering (22).

In previous studies of human parainfluenza virus 3 (HPIV3), an important respiratory pathogen, we have shown that HPIV3 hemagglutinin-neuraminidase (HN) receptor binding protein and F protein interact before and during fusion activation (23). We have proposed that HN contributes to maintaining F in its pretriggered state until the correct time and place for entry, at which time receptor binding switches HN to an active role with respect to activating F and triggers F (23). To address the role of receptor engagement and to elucidate how HN and F interact during fusion, we previously observed the sequence of events leading up to HN/F-mediated membrane fusion in real time, in live cells using bimolecular fluorescent complementation (BiFC), a technique that allows HN-F interactions to be studied under minimally perturbing conditions (19). We determined when and where HN and F interact on the surface of cells prior to and during cell-cell fusion and identified the role of specific sites in HN in mediating the interaction (19). These BiFC results, in combination with other studies of events preceding viral entry, led us to propose a model of how paramyxovirus HN and F mediate fusion during infection (19, 23–27). In this model, HN-F association prior to receptor binding helps stabilize F, preventing its premature activation (19, 28). HN's engagement of receptor molecules drives the formation of HN/F clusters at the site of fusion, and a putative second sialic acid receptor binding site positioned in the dimer interface of HPIV3 HN directly modulates F activation and interaction with F in living cells (7, 19, 24, 29, 30). After initial activation of F, HN and F remain associated and HN acts on F even beyond the step of fusion peptide insertion into the target. As fusion progresses further, either HN and F dissociate or the clusters of HN-F complexes disperse (19).

To evaluate viral surface glycoprotein events of early entry in the context of the virus, we previously conducted a preliminary negative-stain electron tomography (ET) analysis of HPIV3 viral particles that were prepared in the absence of receptors for the virus (28). The majority of viral particles showed fairly continuous coats of glycoprotein spikes with two layers of density that we interpreted to reflect staggered HN and F spikes, in which HN was present in association with prefusion F. Surface density on a subpopulation of small viral particles showed clusters of glycoprotein spikes resembling the crystal structure for postfusion HPIV3 F trimers (31) and the moderate-resolution cryo-negative-stain electron microscopy (EM) reconstruction reported for paramyxovirus SV5 (PIV5) F (4). These observations supported the idea that HN and F are associated on the virion surface prior to receptor engagement.

While a number of other studies have explored paramyxovirus ultrastructure by electron microscopy (32–37), the resolution of surface features has eluded detailed characterization until recently: specifically, the relative distribution, conformation, and interaction of the receptor binding and fusion surface proteins. In a recent study, the use of an engineered measles receptor binding protein (H) with an elongated stalk permitted visualization of the envelope glycoproteins on a virion surface and provided evidence

that direct contact between F and the head domain of H may not be required for activation of measles virus fusion (38).

Challenges of characterizing the surface glycoprotein organization in paramyxoviruses include the multiplicity of conformations HN and F can adopt and the potential for varied interactions between the proteins in different states.

The F protein is generated as a single precursor polypeptide chain that, to be functional, must be cleaved by host proteases into two subunits (F1 and F2), which remain associated (39, 40). The F monomers oligomerize into a squat trimer with a central cavity, giving it a rounded, donut-like appearance from the side and a triangular shape when viewed from above (41, 42). The ectodomain sits on top of a short tether formed by portions of the C-terminal heptad repeat (HRC) segments, which are anchored via the transmembrane domain to the viral membrane. The fusion peptide that corresponds to the N-terminal ~20 residues of the F2 subunit only becomes available to insert into the target membrane once the appropriate trigger for fusion activation is encountered. Once triggered or destabilized, the trimer converts to a more elongated, narrow structure characterized by a stable helical bundle formed by N- and C-terminal heptad repeats (HRN and HRC, respectively). This reorganization colocalizes the two membrane interactive domains, the fusion peptide and the transmembrane anchor. The 3-dimensional structure of the F fusion trimer from multiple paramyxoviruses, including HPIV3, has been described in postfusion forms (31, 43–45).

The several activities of HN—receptor binding, receptor cleaving, fusion activation, and possibly F protein stabilization—are regulated within a type II membrane protein consisting of a cytoplasmic domain, a membrane-spanning region, a stalk region, and a globular head. The stalk confers specificity for the homologous F in the fusion activation process (7, 46–51). Crystal structures of the avian paramyxovirus Newcastle disease virus (NDV) HN (52, 53) and later of the HPIV3 HN (54) and PIV5 HN (55) led to identification of the locations of the primary binding/neuraminidase active site residues on the globular head. For NDV, HPIV1, and HPIV3, a secondary sialic acid binding site on HN plays distinct roles in binding or promoting fusion (7, 19, 24, 30, 53, 56). The relationship of the head and stalk domains in functional paramyxovirus receptor binding proteins remains a critical feature to elucidate because of (i) the role identified for the stalk region in triggering F (7, 12, 57–61) and (ii) the proposed function of the head of the receptor binding protein in both receptor binding and transmitting the activation signal to F (7, 12, 57, 59–62). Receptor binding proteins from various paramyxoviruses have been characterized by crystallography in several conformations and oligomeric forms (29, 46, 54, 55, 63, 64). The evidence suggests that these proteins can adopt at least three arrangements, including a "heads-down" tetramer in which two dimers of HN are organized around a 4-helix stalk (46), a "heads-up" form (55), and a "two-heads-up, two-heads-down" form that has been proposed to represent an intermediate conformation (63). It has been suggested that the head domains of HN in the heads-down configuration are responsible for masking the triggering residues on the stalk region (46, 47).

In order to better define the relationship between HN and F on whole infectious virions prior to receptor engagement and to begin to test models of activation that have emerged from experimental data (1, 2, 8–13, 19, 23, 29), we used a combination of negative-stain and cryo-electron tomography (cryo-ET) here to
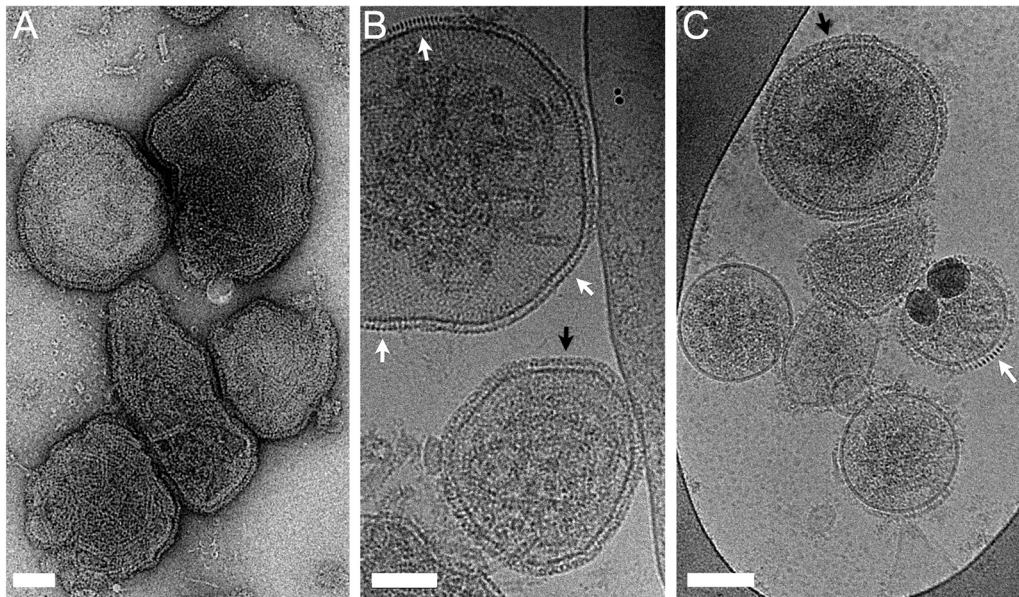
FIG 1 HPIV3 imaged by negative-stain (A) and cryo- (B and C) electron microscopy. As is particularly evident in cryo-electron micrographs, nearly all particles were rounded rather than filamentous in morphology. In addition to a complex, dense layer of surface density (black arrows), regions of ordered density (white arrows) were evident, both attributed to the viral glycoproteins. Scale bars, 100 nm.

image the HPIV3 ultrastructure. We observed that many of the observed surface features are interpretable in terms of known structures for F and HN that have been determined by crystallography and provide information about how the two proteins relate to each other on the surface of virions. The observations of HPIV3 are consistent with a model for fusion in which prefusion F and HN in a heads-up conformation interact prior to receptor engagement, without activating F. Receptor engagement then induces HN to activate F.

RESULTS

HPIV3 particle morphology. As in previously described ultrastructural studies of paramyxoviruses, a high degree of pleomorphy was observed in the population of HPVI3 particles, as examined by both negative-stain and cryo-electron microscopy (Fig. 1) (32–37). Particles ranged from 100 to 500 nm in diameter and were generally rounded in morphology. Filamentous virions were rarely observed in the virus preparations. To obtain a more detailed understanding of virus ultrastructure and to clearly distinguish surface from internal features, we carried out tomographic reconstruction of both negatively stained (Fig. 2; see Movies S1 to S3 in the supplemental material) and cryo-EM specimens (Fig. 3; see Movies S4 to S7 in the supplemental material). Significant ribonucleoprotein (RNP) density was often observed within the majority of particles over 100 nm in diameter, both by negative staining, in cases where stain was able to penetrate into the virions (Fig. 2; see Movies S1 and S2), and by cryo-electron tomography (Fig. 3; see Movies S4 to S7). The number of RNPs packaged appeared to vary substantially across the population. These helical tubes exhibited an average pitch of ~5 nm. They were composed of slanted rings, where each ring segment exhibited an outer diameter of ~18 nm and an inner diameter of ~7 nm (distances measured at half-maximum density). In addition, in some particles with relatively lower internal material density, what appeared to

be actin filaments could be discerned (Fig. 3B); these were more evident in broken particles (see Movie S8 in the supplemental material). The vast majority of particles (~90%) we observed appeared to lack a membrane-associated matrix layer, and those that did exhibit thicker envelopes with an internal matrix layer appeared to be generally smaller particles, sometimes with discernible postfusion F proteins on their surface (Fig. 3C to E) (4, 28). The ratio of matrix-bearing to matrix-lacking particles is similar to what has been observed in other paramyxoviruses (32, 33, 36).

HN tetramers in the heads-down conformation are found in large ordered arrays. In projection images, a variety of complex surface density features were observed on the particles (Fig. 1). In many cases, regularly ordered grid-like patterns of density in the projection images were apparent. Tomographic reconstructions of particles examined by negative-stain and cryo-EM revealed that the grid-like density was located on the virus exterior rather than forming an internal layer such as matrix (Fig. 2A and 3A; see Movies S1 to S7 in the supplemental material). The arrays covered significant areas on the virus surfaces; however, we noted that a high degree of variability in the amount of surface area covered by the arrays was observed; some particles even appeared devoid of the grid-like arrays (Fig. 2B), while others had a majority of their surface covered. The ratio of particles that show the grid-like surface arrays versus those that do not was approximately 2:1; for example, in cryo-electron micrographs, 90 particles showed arrays, while 47 exhibited surfaces without prominent lateral ordering of density. We also observed that multiple arrays with different relative orientations coexisted on different patches of the surface. The arrays were found on both small and large particles, suggesting that surface curvature and overall particle size are not major determinants of array formation (see, for example, Fig. 3C). The ordered, grid-like arrays evident in both negative-stain (Fig. 2 and 4) and cryo-EM (Fig. 3 and 4) images were composed of repeating units of density consistent with the known high-resolution struc-
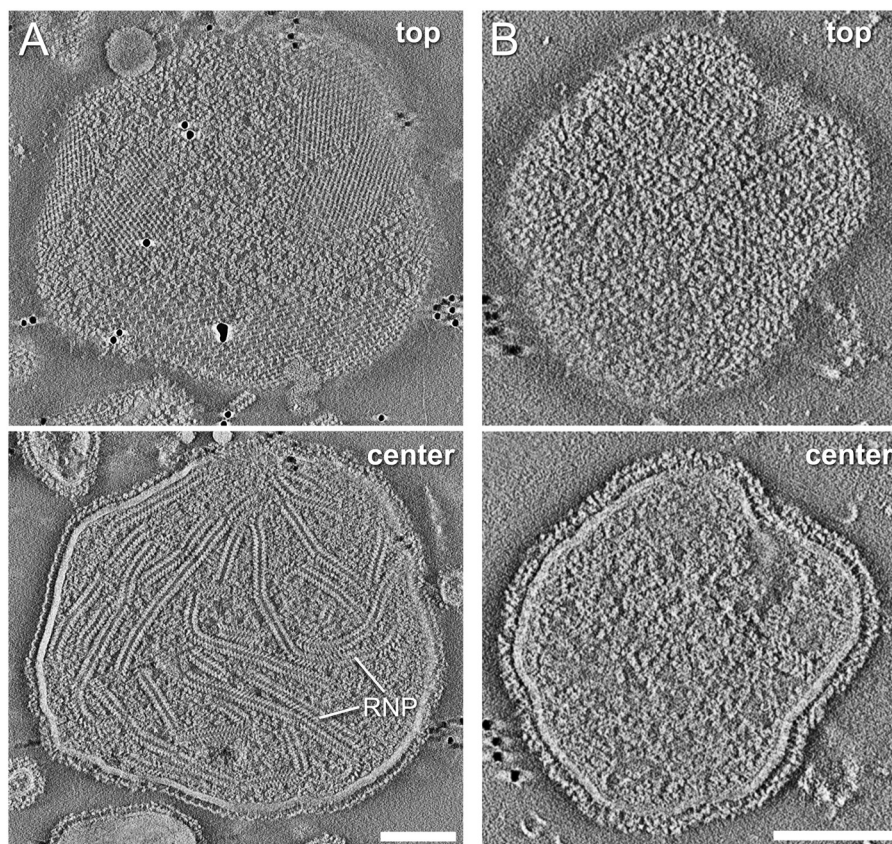
FIG 2 Negative-stain electron tomographic reconstruction of HPVI3 virions. (A) The 4.4-nm-thick slices through the reconstructed density reveal a complex organization of surface features, including ordered arrays of glycoproteins, as well as less regularly ordered proteins, many of which exhibit a triangular shape with stain-penetrable centers. (See Movie S2 in the supplemental material.) The central slice through the particle reveals significant RNP helical tubes inside, as well as lateral views of surface glycoprotein organization. (B) The 2.2-nm-thick slices showing the top of and a central slice through the reconstructed density demonstrate that some particles do not present the grid-like arrays of surface glycoproteins. Instead in these cases, a more complex, double-layer surface appears predominant, as is evident in the edge views of particle central slices. Scale bars, 100 nm.

ture for a tetramer, or dimer of dimers, of NDV HN in the heads-down conformation (Fig. 4) (46). In the negative-stain reconstruction shown in Fig. 4A, sequential slices through the density revealed that the basic unit of the array viewed from above had the form of a slanted "H," which was positioned above punctate dots of density that are consistent with the density for a helical bundle stalk (Fig. 4A; see Fig. S1C in the supplemental material). The tetrameric NDV HN structure (3T1E.pdb) could be docked into the EM density, which shows excellent agreement with the "heads-down" HN conformation (Fig. 4B and C) (46).

Viewed laterally at the edge of a virus particle (Fig. 4C), the HN arrays were observed to flow into repeating rows of Y-shaped density features that correspond to the view of the HN array along the red line shown in Fig. 4B. In other orientations (Fig. 4D), the arrays can be viewed down a different line of sight, as indicated by the blue dashed line in Fig. 4B.

We note that the patches of HN arrays appeared to be composed exclusively of HN in the heads-down conformation; they did not contain density recognizable as F in either postfusion or prefusion conformations.

The HN array density distribution peaks at ~10 nm above the viral membrane (measured from the distance at half-maximum density of the outer leaflet to the peak intensity distal to the mem-

brane) (Fig. 5). This peak density likely corresponds to the neck junction of the HN tetramer, where 3 layers of density from 2 HN head subunit dimers and the tip of the stalk converge (46). The stalk height of 10 nm is the expected height if the complete stalk exists in a helical conformation. Observed from above, the stalks appeared as puncta that are ~4-nm in diameter, consistent with the dimensions expected for a bundle of 4 helices in cross section, as seen in the NDV HN tetramer and stalk domain crystal structures (Fig. 4A; see Fig. S1C in the supplemental material) (46, 47). The arms of the Y feature extended ~12 nm above the outer leaflet (Fig. 5 [measured between distances of half-maximum density at membrane outer leaflet and the distal density peak]) of the viral membrane. The spacings of HN tetramers, measured between stalks center to center, are ~9 nm along one axis of the array and ~14 nm along the other axis. Viewed from above where the dimer of dimers slanted H motif was clearly visible, the edges were 5 nm across and 9 nm long and the distance across the bar of the H was ~11 nm; again corresponding to the NDV heads-down tetramer structure (46). As seen in Fig. 4, tetramers were also staggered row by row rather than being organized in a simple square grid.

In areas without HN arrays, prefusion F is often intermingled with density that may correspond to HN with a heads-up conformation. In most particles, in addition to presenting HN
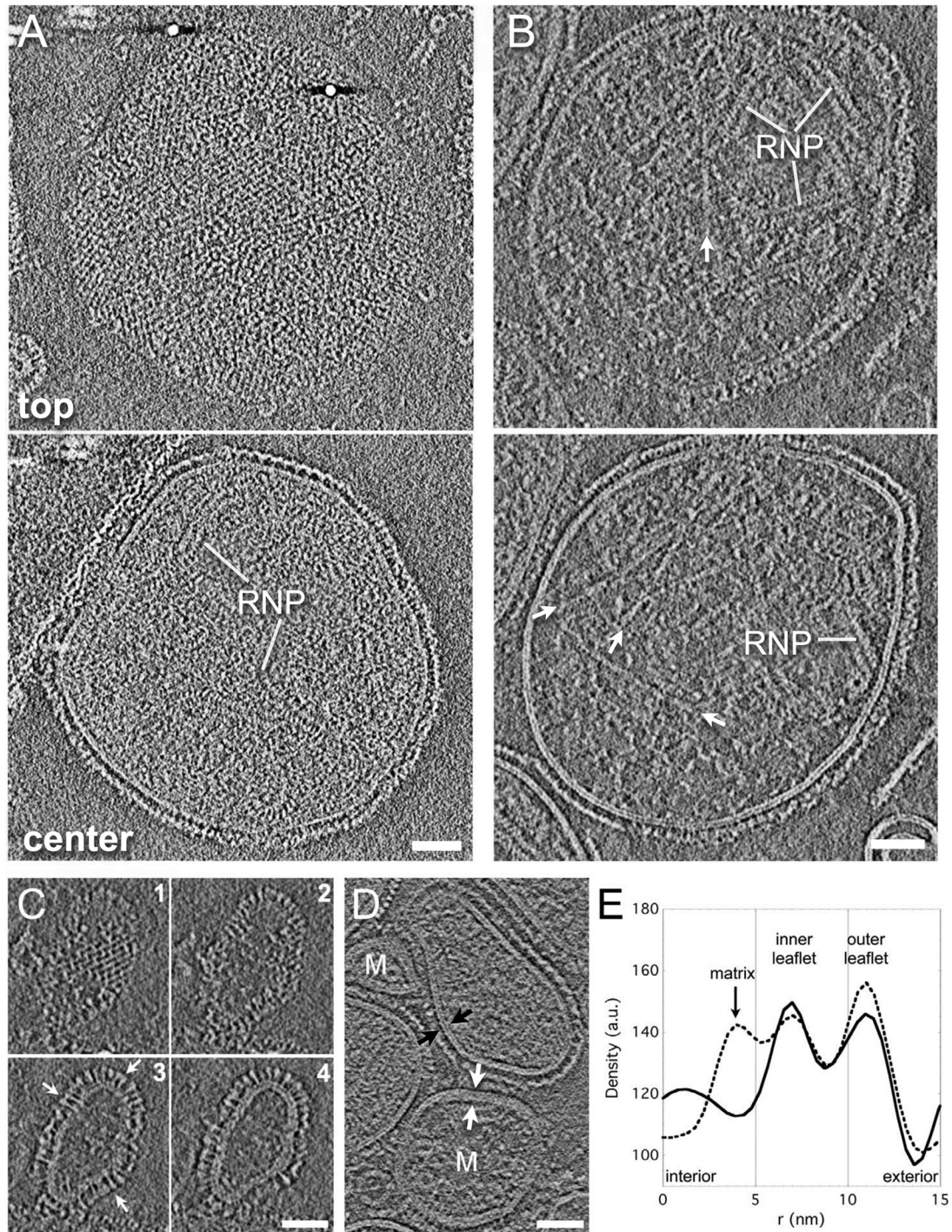
FIG 3 HPIV3 particle ultrastructure imaged by cryo-electron tomography. Shown are 4.4-nm-thick slices of the top and central slices through reconstructed density for two representative HPIV3 particles (A and B). The image gray scale has been inverted for comparison with negative-stain reconstructions, such as in Fig. 2. As with the negatively stained samples, cryo-ET imaging of particles reveal ordered patterns of density on the virus surface, as well as RNP packaged inside (A). In the majority of particles such as in panels A and B, the envelope consisted of simple lipid bilayers with glycoproteins on the exterior; significant spans of membrane-associated density corresponding to an internal matrix layer were not typically observed. (B) In some particles, density consistent with actin filaments is observed inside (white arrows) (75). (C) A few small particles lacking RNP that bear postfusion F (white arrows, upper and lower right edges) and HN arrays were the primary glycoproteins observed on these small particles. (D) Approximately 10% of particles (labeled "M") do appear to exhibit matrix layers that contribute to thicker envelopes. The internal matrix layer is observed ~3 to 4 nm separated from the inner bilayer leaflet (E). a.u., arbitrary units. Scale bars, 50 nm.
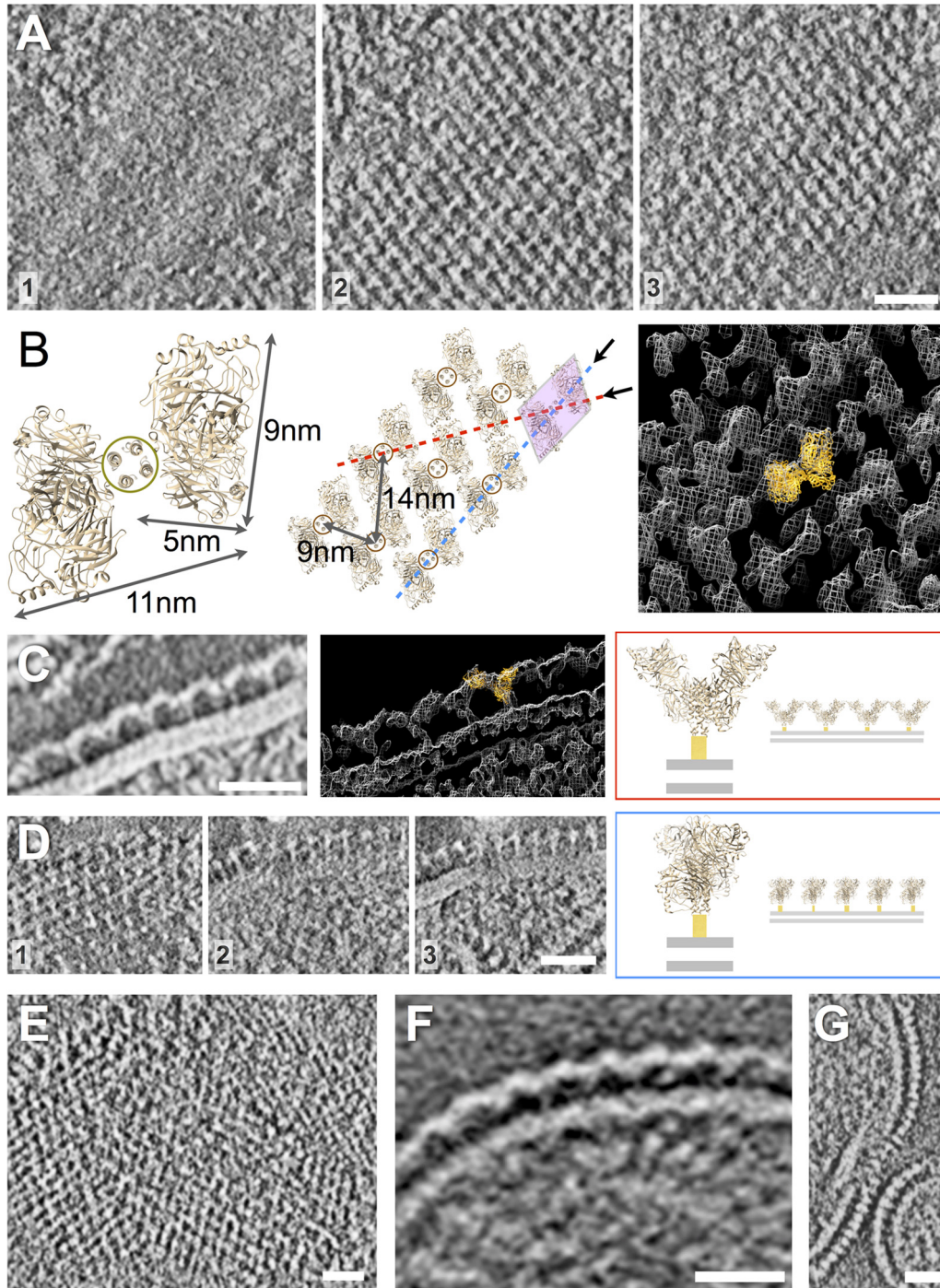
FIG 4 HN arrays imaged by negative-stain electron tomography (A to D) and cryo-electron tomography (E to G). (See Movies S1 to S4, S6, and S7 in the supplemental material.) (A) Serial 3.2-nm slices of a negative-stain tomographic reconstruction, increasing in elevation above the virus surface from left to right (numbered 1 to 3). Viewed from above (slices 2 and 3), this tetramer has a slanted "H" appearance positioned above punctate dots of density that correspond to the tetramer's helical bundle stalk (slice 1). The ordered grids of density on the surface of the virions are composed of repeating units of density, in excellent agreement with the known structure for a tetramer of HN in the heads-down conformation; the crystal structure for NDV HN (3T1E.pdb) is shown for comparison. A model of the array organization based on the crystallographic structure for tetrameric, heads-down HN is shown in panel B and docked (orange ribbon diagram) into the EM density (white mesh). (C) Viewed laterally at the edge of a virus particle, the arrays are observed to flow into repeating rows of Y-shaped density features that correspond to the view of the HN array along the red line shown in panel B. 3T1E.pdb is shown docked into the EM density. (D) In other orientations, the arrays can be viewed down a different axis, indicated by the dashed blue line in panel B; serial slices are ordered from left to right (numbered 1 to 3). Scale bars, 25 nm. (E) Cryo-electron tomographic slice of virion surface shows similar arrays of density as seen from the top of a particle; note that the image gray scale has been inverted for comparison with negative-stain reconstructions above. (F) Y-shaped features are also observed at the edge of particles in central slices. (G) Additional views of the arrays from a different orientation also reveal the regular ordering of surface density. Scale bars, 25 nm.
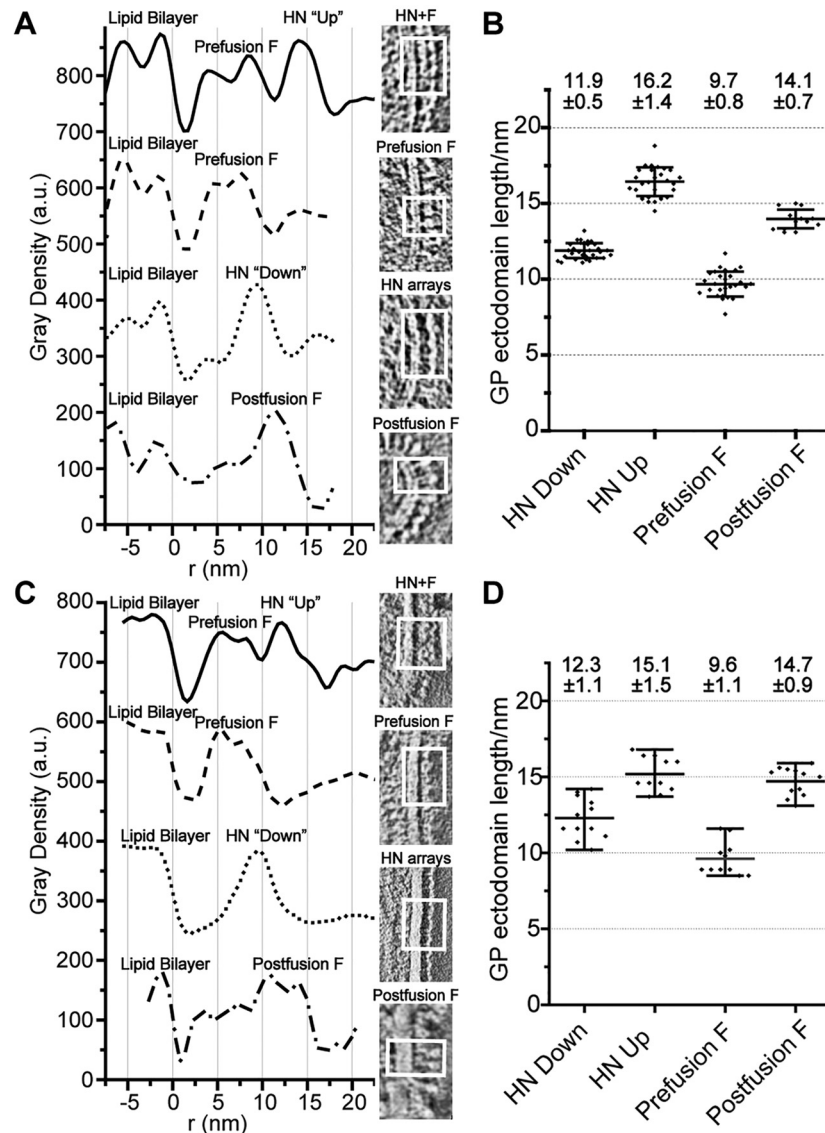
FIG 5 Radial density distribution of surface glycoproteins in different organizations through cryo- and negative-stain electron tomography. (A) Cryo-electron tomography clearly shows the viral lipid bilayer and distinct layers of surface glycoprotein density above the membrane, including double-layered surfaces composed of HN molecules inferred to be in a heads-up configuration adjacent to prefusion F molecules, occasional prefusion F molecules alone, arrays of HN in the heads-down configuration, and postfusion F protein. (B) Measurements of the height of surface glycoproteins from the viral envelope in cryo-ET reconstructions (distances measured from positions of half-maximum density). Numbers indicate average heights ± standard deviations (C and D) Negative-stain electron tomography and height measurements show very similar organizations and good agreement with cryo-ET observations. For additional individual and average measurements, see Fig. S2 in the supplemental material.

heads-down arrays, large portions of the surfaces were covered in a cloak of density that exhibited significant complexity and appeared to be composed of two primary layers of density (Fig. 5 and 6). The double surface layer extended ~16 nm above the virus membrane (Fig. 5). As seen by tomography, the glycoproteins in these complex double layers did not appear to exhibit lateral organization into ordered arrays (Fig. 2B and 6; see Movie S3 in the supplemental material).

The complex double-layered density reflected mixtures of protein types, and while individual glycoproteins were not always discernible, in many instances, prefusion F could be clearly distinguished as the more membrane proximal of the 2 prominent lay-

ers of density (Fig. 6). Indeed, in edge views of central slices through tomograms, the prefusion F trimers were recognized by their squat, rounded shapes with a diameter of ~8.5 nm and central cavities, in excellent agreement with the available crystal structures for prefusion F (e.g., 4GIP.pdb from the related PIV5 [40]), which could readily be docked into the EM density (Fig. 6C) (40–42). The F trimer squats above the membrane, while a discontinuous canopy of density was often observed at higher elevation. In some regions (for example, blue arrows in Fig. 6A), the canopy density was resolved into punctate ~4- to 5-nm-diameter dots that are consistent in size with a globular HN head domain (5 by 4 by 6 nm); the radial density distribution also reflected this distinct 4-
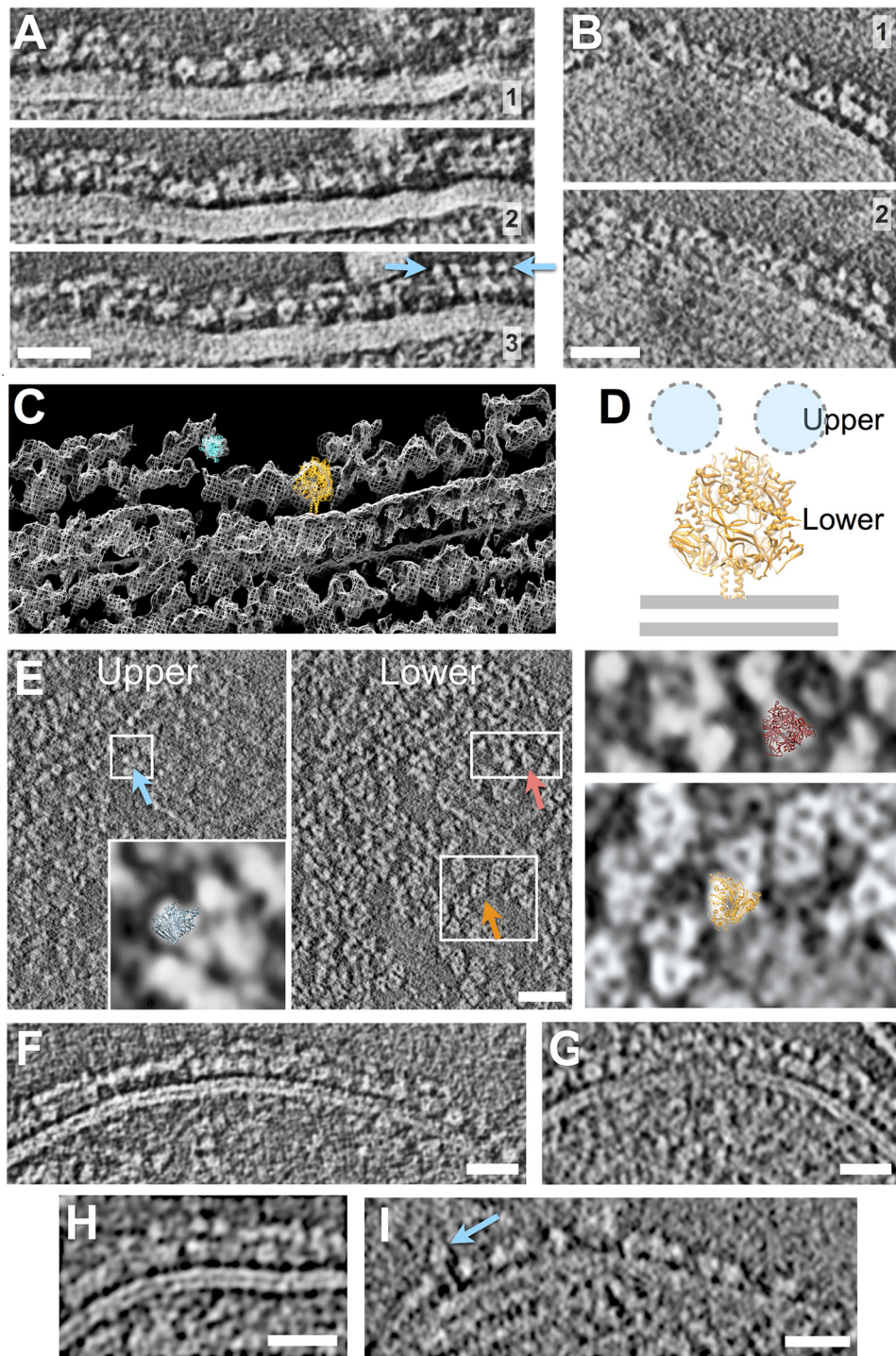
FIG 6 Location of prefusion F trimers on the virus surface. Negative-stain (A to C and E) and cryo- (F to I) electron tomography. Note that for cryo-electron tomograms (F to 1), the image gray scale has been inverted to facilitate comparison with negative-stain reconstructions. The 4.4-nm-thick serial slices showing lateral views of glycoprotein spikes present prefusion F trimers clustered close to the membrane, with additional density features at higher elevations forming a canopy above the F trimers (A and B) interpreted as HN monomers. In some cases, the canopy density is resolved into discrete 4- to 5-nm-diameter puncta (blue arrows in panel A). (C) Crystal structures for prefusion F (orange ribbon diagram; prefusion F from PIV5 4GIP.pdb [40]) docked into the EM density for the globular, donut-like membrane-proximal features, show excellent agreement with EM density, suggesting the organization shown in panel D, with globular HN positioned in the upper layer of density and prefusion F in the lower layer beneath the canopy. (E) The canopy density (4.4-nm-thick "upper" slice) viewed from above shows that, at high elevation, punctate globular density features are observed (blue arrow). For example, the inset shows one HPIV3 HN monomer from 1V2I.pdb [54], blue ribbon diagram, docked into the EM density. In contrast, tightly associated tetramers, as observed in crystal structures of HN head domains from PIV5 (SV5) (1Z4X [55]), were not clearly identifiable. At lower elevations, closer to the virus surface, triangular features consistent with primarily prefusion F are observed (orange arrow). The lower panel on the right shows the 4GIP.pdb prefusion F crystal structure docked into the EM density (40); some instances of smaller-diameter postfusion F trimers are also distinguishable from the prefusion trimers (red arrow). The upper panel on the right shows the HPIV3

(Continued)

to 5 nm-wide feature as the outer density layer (Fig. 5). These outermost globular features themselves were placed atop tethers ~10 to 12 nm above the virus surface. The taller height of these canopy features compared to the shorter heads-down HN tetramer is likely due to the relative positioning of the head and stalk domains in a heads-up configuration. In rare circumstances, what appeared to be individual HN in a heads-up state extending to a height of ~16 nm above the membrane could be seen (Fig. 6I, blue arrow).

In views of top and bottom slices of the reconstructed tomograms for the double surface layer, no evidence was found that suggests other tetrameric organizations of HN, such as the "four-heads-up" state that has been proposed (55, 63). Instead it appeared that the canopy density of HN proximal to F may have been comprised of monomers or dimers of HN. This oligomeric state for HN was not unprecedented as the NDV HN ectodomain, including the stalk domains, yields primarily monomers and dimers in solution, even though dimers of dimers were observed when the constructs were crystallized (46).

Viewed from above by negative-stain ET elevations close to the viral membrane, triangular features with edges ~8.5 nm long that have stain-penetrable central cavities were observed, scattered in an irregular fashion (Fig. 6E, "Lower"). These features are consistent with crystal structures of prefusion F trimers, which are shown docked into the EM density (4GIP.pdb) (orange ribbon diagram in Fig. 6E). In slices of density positioned a few nanometers above these layers (Fig. 6E, "Upper"), we found scattered density, some of which appeared to consist of ~4- to 5-nm dots, sometimes loosely paired; these were similar in dimension and distribution to the globular density features observed in the lateral views of the envelope glycoprotein canopy. Other features seen from this vantage appeared to correspond to F in its postfusion helical bundle state, which appeared as a smaller-dimension triangular feature, with edges ~7 nm long and a spot of stain in its center. The crystal structure for HPIV3 postfusion F could be precisely docked into these density features (1ZTM.pdb) (red ribbon diagram in Fig. 6E) (31). Many of these smaller triangles had electron-dense stalks beneath them that were ~2.5 nm in diameter, consistent in dimension with the helical bundles formed by the HRN and HRC domains in postfusion F (see Fig. S1 in the supplemental material) (31). Prefusion F trimers are also observed in clusters adjacent to each other, in some cases without clear signs of associated HN (Fig. 6I). In lateral views at the edge of particles observed in central slices, the distinction of prefusion and postfusion F, as well as the double-layered surface density, were clearly evident (see Fig. S2 in the supplemental material).

In cryo-EM reconstructions, due to the need to work at higher defocus values and because the particles were more rounded rather than flattened in the negative-stain case, views of trimers down their axis of symmetry were rarer. However, in lateral views seen in central tomographic slices, the regions of the virus surface with two layers of external density were evident just as with the negative-stained samples (Fig. 6F to I). In addition, the positioning and radial density distribution of surface density features were

found to be similar by cryo- and negative-stain EM (Fig. 5). Thus, the overall surface glycoprotein organizations analyzed by cryo- and negative-stain EM are in good agreement.

The EM observations and comparison with crystal structures suggest that prefusion F is present in fields interspersed with copies of what we infer to be HN in a nonarrayed, heads-up form that gives rise to the canopy of density.

DISCUSSION

The electron tomography studies reported here provide images of glycoprotein organization on the surface of HPIV3. When taken together with our experimental data, the structural information begins to elucidate features of glycoprotein interaction that are relevant to viral entry. Many of the observed surface characteristics are interpretable in terms of known structures for F and HN that have been determined by crystallography, and we now can identify how the two types of proteins relate to each other and are distributed on the virus surface (summarized in Fig. 7A).

HN in its heads-down conformation is not associated with F. One striking feature seen in the tomographic reconstructions were the arrays of HN in a tetrameric, dimer-of-dimers, heads-down conformation, showing that the structure observed by crystallography of the isolated NDV HN tetramer exists on the surface at least of some paramyxoviruses. These arrays did not appear to contain F; in fact, F is not observed in association with a heads-down HN. Furthermore, in this conformation, none of the sialic acid binding sites was oriented to face the target membrane, and only two out of the four HN head domains would be proximal to the target membrane, while the other two have been proposed to be engaged in interactions with the HN stalk and to be sequestered from interacting with the receptors on the target membrane (46). For another paramyxovirus, Newcastle disease virus (NDV), our experimental data suggested two active sites on NDV HN, where site I exhibits both neuraminidase and receptor binding activity and site II possesses only the receptor binding function (30). These two sites were also identified in the X-ray crystal structures of NDV HN (46, 53). We found that engagement of NDV's site I with the receptor leads to the activation of site II and promotion of fusion (30). It has been suggested that during interaction with sialic acid receptors on the target cell membrane, the head domains may reorient to further expose the other head domains (46). For HPIV3, we showed that a second putative sialic acid binding site on HN modulates HN-HN dimerization and F triggering by HPIV3 HN (7, 19, 24). The finding that HPIV3 F is not observed in association with a heads-down HN on the virus surface implies that for the HN-F association to occur, the HN heads must be "up." Future experiments will address the question of whether heads-down HN molecules without associated F molecules are available for receptor engagement.

HN in a heads-up conformation on the virus surface is colocalized with prefusion F. In the regions of the virus surface that exhibit double layers of density, we observed a tall canopy of density above prefusion F trimers that we infer to be HN in a different conformation from the heads-down tetramer. This canopy den-

Figure Legend Continued
postfusion F trimer, 1ZTM.pdb, docked into the EM density (31). (See Fig. S1 in the supplemental material.) (F to I) Central slices of cryo-electron tomography showing lateral views of F protein distribution on the virus surface. In some cases, isolated prefusion F trimers are observed (I), while in other cases (F to H), prefusion F is found in regions of double-layer surface density, positioned beneath a discontinuous canopy of density we infer to be HN. Scale bars, 25 nm.
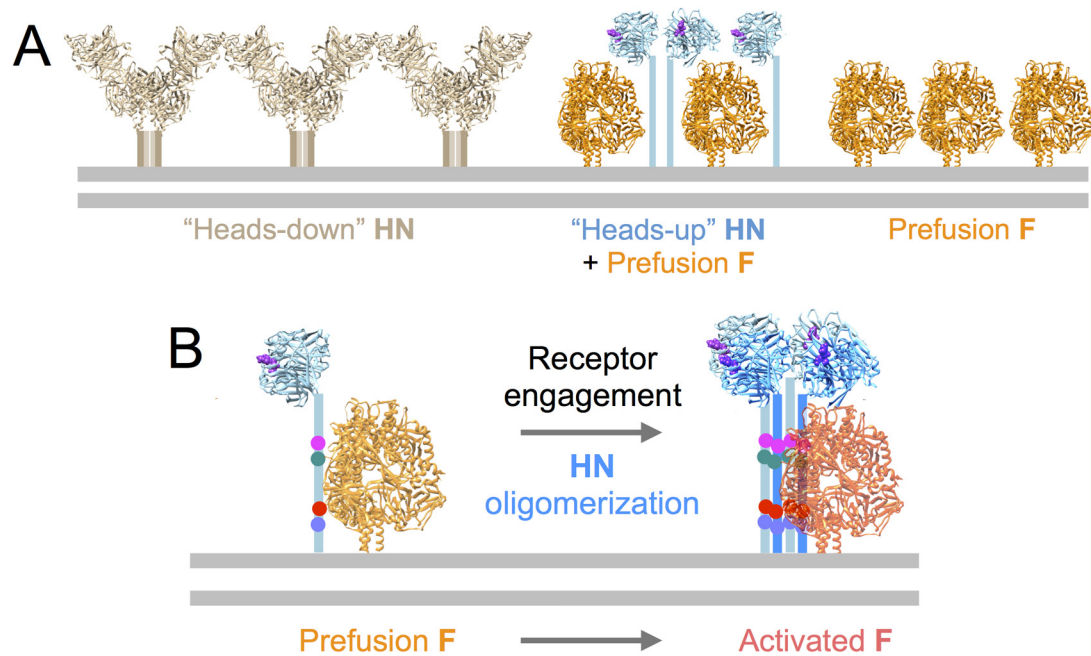
FIG 7 Implications for fusion triggering and HN-F interactions. Observation of viral surfaces in the absence of receptor engagement include HN tetramers in the heads-down configuration in arrays on the virus surface. These heads-down tetramers were not observed in association with F. On these virions without receptor engagement, some prefusion F is interspersed with HN in an extended configuration with the globular heads towering above the level of the F consistent with a heads-up but monomeric or dimeric form. F alone is also observed in both the prefusion and postfusion forms. The data support the notion that F and HN are clustered with each other prior to receptor engagement by HN and that the presence of a heads-up form of HN in proximity to prefusion F is not sufficient to induce F activation. (B) Since tetrameric, heads-up HN was not observed either alone or in association with F, the possibility exists that oligomerization induced by receptor engagement (not studied here) is important for triggering F.

sity appears to be attributable to a heads-up conformation of HN with loosely associated head domain dimers or possibly monomers atop an extended stalk. We did not observe clearly ordered density that would be consistent with HN tetramers in a heads-up configuration, a conformation that was proposed based on a crystal structure for the SV5 HN head domain (55). It should be noted that little evidence exists to indicate that the HN head domains themselves adopt a tightly organized heads-up tetramer in the absence of a tetramerized stalk domain. The tetrameric, heads-up model was based upon a crystal structure for heads only, lacking the tethers (55), and may not represent the physiological assembly of HN that triggers F. HN head domains lacking the stalk regions, from various paramyxoviruses, rarely form tetramers in solution. HPVI3 HN head domains crystallized as a dimer (29, 54), and the head domain of NDV and of the model paramyxovirus SV5 (PIV5) are monomeric in solution, while the introduction of the stalk domain can in part facilitate tetramerization (65). The helical stalk region of PIV5 has a propensity to form 4-helix bundles (47, 65), while NDV HN has a lower propensity to form a tetramer (47). It has been proposed that specific residues that face the helical bundle's hydrophobic core in PIV5 are substituted for by polar residues in NDV, possibly hindering the putative stalk-driven receptor binding protein tetramerization (65).

We have previously shown that association of HN with F stabilizes F in its prefusion conformation under experimental conditions, making it less readily activated by heat, and that in live cells, HN and F are associated with each other prior to receptor engagement (19, 28, 66). The observation of some clusters of prefusion F trimers on the virus surface shown in Fig. 6, without detectable

glycoprotein "chaperone" such as HN in close contact, suggests that under the conditions of this experiment, prefusion F might exist without close association or coordination with HN. However, in light of the biological data provided by BiFC showing association of HN and F expressed on cells (19, 29) and the biochemical evidence for stabilization of F by HN (28), the presence of prefusion F alone does not distinguish between the models of fusion. While under certain conditions HN stabilizes F in its prefusion state, it has not yet been possible to determine under which *in vivo* circumstances HN provides a direct stabilizing role. Ongoing studies to capture F during serial steps of entry should be informative with respect to this functional question and will also determine whether similar glycoprotein organizations are present in viruses isolated from natural infections.

In a previous study, lower-resolution negative-stain images and density distributions, compared to crystal structures, suggested that HN and F were colocalized in some HPIV3 particles absent receptor engagement, giving rise to the double layers (28). These observations supported our biochemical and BiFC evidence for the association of HN and F prior to HN's receptor engagement (19). The higher-resolution cryo- and negative-stain data in the present report provide considerably more detail about the relationship and conformations of HN and F on the surface of HPIV3. Prefusion F and HN in a heads-up state can intermingle and combine to form the double layers of density on the virus surface in the absence of receptor engagement, with prefusion F trimers situated beneath the canopy formed by what appears to be mostly monomeric or dimeric HN. The available data cannot explain whether in the colocalized state, HN and F interact strongly

and are specifically associated or whether they are simply clustered in the same vicinity.

Oligomerization and implications of imaging results for activation of fusion. A body of biochemical and virological data now support an important role for HN in triggering the F protein's fusion activation (1, 2, 6–13, 19, 26, 67). Specific residues on the stalk domain have been implicated in triggering F protein activation in HPIV3 and related paramyxoviruses (47, 61). While the relevant HPIV3 HN stalk residues in extended conformations would likely be exposed and available to interact with nearby F molecules in the double-layered regions we observed, the exposure of the stalks of the heads-up HN does not appear sufficient to activate F. It may be necessary for the stalk domains to oligomerize (such as into helical bundles) in order to present the proper quaternary spatial organization of residues in order for HN to bind receptor and to trigger F (Fig. 7B). This notion is supported by our BiFC experiments, in which clusters of HN and F form upon receptor engagement (19, 29). We have proposed (19) that the switch of HN to an F-activating role is mediated by HN binding to the receptor; receptor engagement may encourage oligomerization of HN subunits into functional dimers or perhaps tetramers, leading to F activation (19). For Sendai virus, it has been observed that the tetrasialylated GQ1b ganglioside induces fusion far more efficiently than the disialylated GD1a (68). Likewise, in studies of fusion activation by headless forms of measles virus H protein, while in the presence of specific stalk mutations, the head was shown to be dispensable: a tetramerization motif was required for the mutated stalk in order to produce efficient F activation (38). Nipah receptor binding protein (G) lacking a head was shown to be capable of activating F, potentially implying that receptor engagement by the head is dispensable; however, only a small subset of such proteins with a specific stalk length could do so (69), and it seems that only those specific stalks could circumvent the requirement for head engagement. For HPIV3, we showed that mutations affecting HN dimerization also impact F activation and fusion efficiency (29); reductions in monomer-monomer interaction led to decreased fusion promotion. Thus, HN oligomerization properties have a role in modulating HPIV3 F protein activation, and the HN/F clustering that follows interaction with cell surface receptors (19) may help promote the formation of a tetrameric or higher-order helical bundle in the stalk domain (Fig. 7B).

An alternative but not necessarily mutually exclusive model (sometimes referred to as the "provocateur" model) proposes that receptor engagement triggers HN to undergo a switch from a heads-down to heads-up configuration, leading to exposure of an F-interactive motif on the HN stalk region (1). If this mechanism is in play, the arrays of HN with the heads-down conformation would need to be disrupted upon receptor binding in order to transition to the proposed HN heads-up conformation that can interact with and activate F (55, 63); however, our observation of heads-up HN associated with F prior to receptor engagement does not appear to be consistent with the purely provocateur model for HPIV3. Future experiments may help determine whether—in concert with receptor avidity-driven oligomerization of HN—a heads-down to heads-up transition could contribute to conversion of significant levels of HN to an F-activatable form.

These data provide evidence in support of several proposed steps in viral entry into cells. Prefusion F is colocalized with heads-up HN prior to receptor engagement by HN, indicating that at least the observed heads-up form of HN does not by itself provide sufficient stimulus for F activation. Instead, as suggested by experiments in live cells (19), receptor engagement likely provides the activation signal necessary to trigger F. The tomography approach here lacks sufficient resolution to determine which parts of F may interact with the HN stalk and head domains. Complementary methods are needed to determine how the various functions of HN are regulated in real time. These questions await experiments that are under way to synchronize and capture individual intermediates in the process. Given that clinically infectious viruses have a balance of fusion properties different from laboratory isolates (29, 70), it will be important to also examine viruses that are infectious *in vivo*. Preliminary EM observations of HPIV3 clinical isolates indicate that the structures observed in this study for the laboratory reference strains of HPIV3 are conserved in the viruses circulating as human pathogens (A.M. and M.P., unpublished data). In future studies, the approach presented here may also help to reveal the changes in the paramyxovirus fusion machinery that are induced by receptor binding.

MATERIALS AND METHODS

Virus growth and purification. CV-1 cells (in 70 to 90% confluent monolayers) in T175 flasks were infected with HPIV3 (multiplicity of infection of 0.1) in 10 ml Opti-MEM (L-glutamine and HEPES) for 90 min in a 37°C humidified, 5% CO_2 incubator. During the 90 min of incubation, flasks were gently shaken every 15 min. Viral inocula were replaced with 20 ml of complete medium with or without neuraminidase to deplete receptors for HN, and cultures were placed in a 37°C humidified, 5% CO_2 incubator. After 48 h, the cell culture supernatant fluid was collected and clarified by centrifugation (3,000 rpm for 10 min at 4°C in an Eppendorf 5810R). The clarified supernatant fluid was centrifuged (25,000 rpm for 120 min at 4°C in an SW28 rotor, Beckman L8-80M ultracentrifuge) through an 8-ml 20% (wt/vol) sucrose cushion in phosphate-buffered saline (PBS) (pH 7.4) or in PBS containing 1 mM zanamivir (pH 7.4) to prevent receptor engagement by HN. Pellets were resuspended in 200 μl of PBS with or without zanamivir (4°C, pH 7.4) for each T175 flask. Virus stocks were stored at −80°C or kept at 4°C before analysis. The titers of HPIV3 stocks were determined by a plaque assay performed as described before (24). Titers for purified viruses after storage at −80°C were 1.00×10^7 PFU/ml.

Negative-stain and cryo-electron tomography. Purified HPIV3 produced as described above was mixed with 10-nm-particle-size colloidal gold and prepared for cryo-electron tomography by addition of 3 μl of sample onto holey carbon-coated grids (C-flat, 200 mesh; Electron Microscopy Sciences) and plunge freezing the samples in liquid ethane using a Vitrobot (Mark IV; FEI Co.). Negative-staining grids were prepared similarly by loading 3 μl of samples onto carbon-coated electron microscope grids (300 mesh; Electron Microscopy Sciences) and stained with nano-W (2% methylamine tungstate; Nanoprobes). Vitrified grids were imaged at liquid nitrogen temperature in a FEI Tecnai F20 transmission electron microscope equipped with a Gatan Ultrascan 4000 charge-coupled device (CCD) camera. Images were captured at a magnification of 25,000× and binned by a factor of 2, giving a pixel size of 4.4 Å in the specimen. Images were acquired at 2 to 4 μm underfocus, and specimens were tilted in 2° steps from approximately 58° to −58° using the Leginon software package (71). The total electron dosage for the entire tilt series was estimated at ~100 e/Å2 per tilt series. Tomograms were reconstructed using the weighed back-projection method in the IMOD package (72). Images were visualized in ImageJ and denoised as previously described (73).

Crystal structures for prefusion F trimer (4GIP.pdb) (40), postfusion F trimer (1ZTM.pdb) (31), heads-down tetrameric HN from NDV (3T1E.pdb) (46), and the globular head domain from HPIV3 HN (1V2I.pdb) (54) were docked into 3-dimensional reconstructed EM density maps that had been denoised by Gaussian filtering and using the "Hide Dust" function in Chimera (74). The automated "Fit to Map" func-

tion was used following initial manual placement of the Protein Data Bank (PDB) model into the EM density map.

REFERENCES

1. Jardetzky TS, Lamb RA. 2014. Activation of paramyxovirus membrane fusion and virus entry. Curr Opin Virol 5:24–33. http://dx.doi.org/10.1016/j.coviro.2014.01.005.

2. Plattet P, Plemper RK. 2013. Envelope protein dynamics in paramyxovirus entry. mBio 4(4):e00413-13. http://dx.doi.org/10.1128/mBio.00413-13.

3. White JM, Delos SE, Brecher M, Schornberg K. 2008. Structures and mechanisms of viral membrane fusion proteins: multiple variations on a common theme. Crit Rev Biochem Mol Biol 43:189–219. http://dx.doi.org/10.1080/10409230802058320.

4. Ludwig K, Schade B, Böttcher C, Korte T, Ohlwein N, Baljinnyam B, Veit M, Herrmann A. 2008. Electron cryomicroscopy reveals different F1+F2 protein states in intact parainfluenza virions. J Virol 82:3775–3781. http://dx.doi.org/10.1128/JVI.02154-07.

5. Moscona A, Peluso RW. 1991. Fusion properties of cells persistently infected with human parainfluenza virus type 3: participation of hemagglutinin-neuraminidase in membrane fusion. J Virol 65:2773–2777.

6. Moscona A, Peluso RW. 1993. Relative affinity of the human parainfluenza virus 3 hemagglutinin-neuraminidase for sialic acid correlates with virus-induced fusion activity. J Virol 67:6463–6468.

7. Porotto M, Murrell M, Greengard O, Moscona A. 2003. Triggering of human parainfluenza virus 3 fusion protein (F) by the hemagglutinin-neuraminidase (HN): an HN mutation diminishing the rate of F activation and fusion. J Virol 77:3647–3654. http://dx.doi.org/10.1128/JVI.77.6.3647-3654.2003.

8. Iorio RM, Melanson VR, Mahon PJ. 2009. Glycoprotein interactions in paramyxovirus fusion. Future Virol 4:335–351. http://dx.doi.org/10.2217/fvl.09.17.

9. Chang A, Dutch RE. 2012. Paramyxovirus fusion and entry: multiple paths to a common end. Viruses 4:613–636. http://dx.doi.org/10.3390/v4040613.

10. Steffen DL, Xu K, Nikolov DB, Broder CC. 2012. Henipavirus mediated membrane fusion, virus entry and targeted therapeutics. Viruses 4:280–309. http://dx.doi.org/10.3390/v4020280.

11. Vigant F, Lee B. 2011. Hendra and Nipah infection: pathology, models and potential therapies. Infect Disord Drug Targets 11:315–336. http://dx.doi.org/10.2174/187152611795768097.

12. Navaratnarajah CK, Negi S, Braun W, Cattaneo R. 2012. Membrane fusion triggering: three modules with different structure and function in the upper half of the measles virus attachment protein stalk. J Biol Chem 287:38543–38551. http://dx.doi.org/10.1074/jbc.M112.410563.

13. Mateo M, Navaratnarajah CK, Cattaneo R. 2014. Structural basis of efficient contagion: measles variations on a theme by parainfluenza viruses. Curr Opin Virol 5:16–23. http://dx.doi.org/10.1016/j.coviro.2014.01.004.

14. Lamb RA, Paterson RG, Jardetzky TS. 2006. Paramyxovirus membrane fusion: lessons from the F and HN atomic structures. Virology 344:30–37. http://dx.doi.org/10.1016/j.virol.2005.09.007.

15. Li J, Quinlan E, Mirza A, Iorio RM. 2004. Mutated form of the Newcastle disease virus hemagglutinin-neuraminidase interacts with the homologous fusion protein despite deficiencies in both receptor recognition and fusion promotion. J Virol 78:5299–5310. http://dx.doi.org/10.1128/JVI.78.10.5299-5310.2004.

16. Harrison SC. 2008. Viral membrane fusion. Nat Struct Mol Biol 15:690–698. http://dx.doi.org/10.1038/nsmb.1456.

17. Plemper RK, Brindley MA, Iorio RM. 2011. Structural and mechanistic studies of measles virus illuminate paramyxovirus entry. PLoS Pathog 7:e1002058. http://dx.doi.org/10.1371/journal.ppat.1002058.

18. Smith EC, Popa A, Chang A, Masante C, Dutch RE. 2009. Viral entry mechanisms: the increasing diversity of paramyxovirus entry. FEBS J 276:7217–7227. http://dx.doi.org/10.1111/j.1742-4658.2009.07401.x.

19. Porotto M, Palmer SG, Palermo LM, Moscona A. 2012. Mechanism of fusion triggering by human parainfluenza virus type III: communication between viral glycoproteins during entry. J Biol Chem 287:778–793. http://dx.doi.org/10.1074/jbc.M111.298059.

20. Corey EA, Iorio RM. 2007. Mutations in the stalk of the measles virus hemagglutinin protein decrease fusion but do not interfere with virus-specific interaction with the homologous fusion protein. J Virol 81:9900–9910. http://dx.doi.org/10.1128/JVI.00909-07.

21. Mirza AM, Aguilar HC, Zhu Q, Mahon PJ, Rota PA, Lee B, Iorio RM. 2011. Triggering of the Newcastle disease virus fusion protein by a chimeric attachment protein that binds to Nipah virus receptors. J Biol Chem 286:17851–17860. http://dx.doi.org/10.1074/jbc.M111.233965.

22. Ader N, Brindley M, Avila M, Örvell C, Horvat B, Hiltensperger G, Schneider-Schaulies J, Vandevelde M, Zurbriggen A, Plemper RK, Plattet P. 2013. Mechanism for active membrane fusion triggering by morbillivirus attachment protein. J Virol 87:314–326. http://dx.doi.org/10.1128/JVI.01826-12.

23. Porotto M, Devito I, Palmer SG, Jurgens EM, Yee JL, Yokoyama CC, Pessi A, Moscona A. 2011. Spring-loaded model revisited: paramyxovirus fusion requires engagement of a receptor binding protein beyond initial triggering of the fusion protein. J Virol 85:12867–12880. http://dx.doi.org/10.1128/JVI.05873-11.

24. Palmer SG, Porotto M, Palermo LM, Cunha LF, Greengard O, Moscona A. 2012. Adaptation of human parainfluenza virus to airway epithelium reveals fusion properties required for growth in host tissue. mBio 3(3):e00137-12. http://dx.doi.org/10.1128/mBio.00137-12.

25. Porotto M, Salah Z, Devito I, Talekar A, Palmer SG, Xu R, Wilson IA, Moscona A. 2012. The second receptor binding site of the globular head of the Newcastle disease virus (NDV) hemagglutinin-neuraminidase activates the stalk of multiple paramyxovirus receptor binding proteins to trigger fusion. J Virol 86:5730–5741. http://dx.doi.org/10.1128/JVI.06793-11.

26. Farzan SF, Palermo LM, Yokoyama CC, Orefice G, Fornabaio M, Sarkar A, Kellogg GE, Greengard O, Porotto M, Moscona A. 2011. Premature activation of the paramyxovirus fusion protein before target cell attachment with corruption of the viral fusion machinery. J Biol Chem 286:37945–37954. http://dx.doi.org/10.1074/jbc.M111.256248.

27. Porotto M, Rockx B, Yokoyama CC, Talekar A, Devito I, Palermo LM, Liu J, Cortese R, Lu M, Feldmann H, Pessi A, Moscona A. 2010. Inhibition of Nipah virus infection in vivo: targeting an early stage of paramyxovirus fusion activation during viral entry. PLoS Pathog. 6:e1001168. http://dx.doi.org/10.1371/journal.ppat.1001168.

28. Porotto M, Salah ZW, Gui L, Devito I, Jurgens EM, Lu H, Yokoyama CC, Palermo LM, Lee KK, Moscona A. 2012. Regulation of paramyxovirus fusion activation: the hemagglutinin-neuraminidase protein stabilizes the fusion protein in a pretriggered state. J Virol 86:12838–12848. http://dx.doi.org/10.1128/JVI.01965-12.

29. Xu R, Palmer SG, Porotto M, Palermo LM, Niewiesk S, Wilson IA, Moscona A. 2013. Interaction between the hemagglutinin-neuraminidase and fusion glycoproteins of human parainfluenza virus type III regulates viral growth in vivo. mBio 4(5):e00803-13. http://dx.doi.org/10.1128/mBio.00803-13.

30. Porotto M, Fornabaio M, Greengard O, Murrell MT, Kellogg GE, Moscona A. 2006. Paramyxovirus receptor-binding molecules: engagement of one site on the hemagglutinin-neuraminidase protein modulates

activity at the second site. J Virol **80:**1204–1213. http://dx.doi.org/10.1128/JVI.80.3.1204-1213.2006.

31. **Yin HS, Paterson RG, Wen X, Lamb RA, Jardetzky TS.** 2005. Structure of the uncleaved ectodomain of the paramyxovirus (hPIV3) fusion protein. Proc Natl Acad Sci U S A **102:**9288–9293. http://dx.doi.org/10.1073/pnas.0503989102.

32. **Liljeroos L, Huiskonen JT, Ora A, Susi P, Butcher SJ.** 2011. Electron cryotomography of measles virus reveals how matrix protein coats the ribonucleocapsid within intact virions. Proc Natl Acad Sci U S A **108:**18085–18090. http://dx.doi.org/10.1073/pnas.1105770108.

33. **Liljeroos L, Krzyzaniak MA, Helenius A, Butcher SJ.** 2013. Architecture of respiratory syncytial virus revealed by electron cryotomography. Proc Natl Acad Sci U S A **110:**11133–11138. http://dx.doi.org/10.1073/pnas.1309070110.

34. **Kiss G, Holl JM, Williams GM, Alonas E, Vanover D, Lifland AW, Gudheti M, Guerrero-Ferreira RC, Nair V, Yi H, Graham BS, Santangelo PJ, Wright ER.** 2014. Structural analysis of respiratory syncytial virus reveals the position of M2-1 between the matrix protein and the ribonucleoprotein complex. J Virol **88:**7602–7617. http://dx.doi.org/10.1128/JVI.00256-14.

35. **Terrier O, Rolland JP, Rosa-Calatrava M, Lina B, Thomas D, Moules V.** 2009. Parainfluenza virus type 5 (PIV-5) morphology revealed by cryo-electron microscopy. Virus Res **142:**200–203. http://dx.doi.org/10.1016/j.virusres.2008.12.017.

36. **Battisti AJ, Meng G, Winkler DC, McGinnes LW, Plevka P, Steven AC, Morrison TG, Rossmann MG.** 2012. Structure and assembly of a paramyxovirus matrix protein. Proc Natl Acad Sci U S A **109:**13996–14000. http://dx.doi.org/10.1073/pnas.1210275109.

37. **Loney C, Mottet-Osman G, Roux L, Bhella D.** 2009. Paramyxovirus ultrastructure and genome packaging: cryo-electron tomography of Sendai virus. J Virol **83:**8191–8197. http://dx.doi.org/10.1128/JVI.00693-09.

38. **Brindley MA, Suter R, Schestak I, Kiss G, Wright ER, Plemper RK.** 2013. A stabilized headless measles virus attachment protein stalk efficiently triggers membrane fusion. J Virol **87:**11693–11703. http://dx.doi.org/10.1128/JVI.01945-13.

39. **Thompson-Wicking K, Francis RW, Stirnweiss A, Ferrari E, Welch MD, Baker E, Murch AR, Gout AM, Carter KW, Charles AK, Phillips MB, Kees UR, Beesley AH.** 2013. Novel BRD4-NUT fusion isoforms increase the pathogenic complexity in NUT midline carcinoma. Oncogene **32:**4664–4674. http://dx.doi.org/10.1038/onc.2012.487.

40. **Welch BD, Liu Y, Kors CA, Leser GP, Jardetzky TS, Lamb RA.** 2012. Structure of the cleavage-activated prefusion form of the parainfluenza virus 5 fusion protein. Proc Natl Acad Sci U S A **109:**16672–16677. http://dx.doi.org/10.1073/pnas.1213802109.

41. **McLellan JS, Chen M, Leung S, Graepel KW, Du X, Yang Y, Zhou T, Baxa U, Yasuda E, Beaumont T, Kumar A, Modjarrad K, Zheng Z, Zhao M, Xia N, Kwong PD, Graham BS.** 2013. Structure of RSV fusion glycoprotein trimer bound to a prefusion-specific neutralizing antibody. Science **340:**1113–1117. http://dx.doi.org/10.1126/science.1234914.

42. **Yin HS, Wen X, Paterson RG, Lamb RA, Jardetzky TS.** 2006. Structure of the parainfluenza virus 5-F protein in its metastable, prefusion conformation. Nature **439:**38–44. http://dx.doi.org/10.1038/nature04322.

43. **McLellan JS, Yang Y, Graham BS, Kwong PD.** 2011. Structure of respiratory syncytial virus fusion glycoprotein in the postfusion conformation reveals preservation of neutralizing epitopes. J Virol **85:**7788–7796. http://dx.doi.org/10.1128/JVI.00555-11.

44. **Swanson K, Wen X, Leser GP, Paterson RG, Lamb RA, Jardetzky TS.** 2010. Structure of the Newcastle disease virus F protein in the post-fusion conformation. Virology **402:**372–379. http://dx.doi.org/10.1016/j.virol.2010.03.050.

45. **Wen X, Krause JC, Leser GP, Cox RG, Lamb RA, Williams JV, Crowe JE, Jr, Jardetzky TS.** 2012. Structure of the human metapneumovirus fusion protein with neutralizing antibody identifies a pneumovirus antigenic site. Nat Struct Mol Biol **19:**461–463. http://dx.doi.org/10.1038/nsmb.2250.

46. **Yuan P, Swanson KA, Leser GP, Paterson RG, Lamb RA, Jardetzky TS.** 2011. Structure of the Newcastle disease virus hemagglutinin-neuraminidase (HN) ectodomain reveals a four-helix bundle stalk. Proc Natl Acad Sci U S A **108:**14920–14925. http://dx.doi.org/10.1073/pnas.1111691108.

47. **Bose S, Welch BD, Kors CA, Yuan P, Jardetzky TS, Lamb RA.** 2011. Structure and mutagenesis of the parainfluenza virus 5 hemagglutinin-neuraminidase stalk domain reveals a four-helix bundle and the role of the

48. **Deng R, Wang Z, Mirza AM, Iorio RM.** 1995. Localization of a domain on the paramyxovirus attachment protein required for the promotion of cellular fusion by its homologous fusion protein spike. Virology **209:**457–469. http://dx.doi.org/10.1006/viro.1995.1278.

49. **Sergel T, McGinnes LW, Peeples ME, Morrison TG.** 1993. The attachment function of the Newcastle disease virus hemagglutinin-neuraminidase protein can be separated from fusion promotion by mutation. Virology **193:**717–726. http://dx.doi.org/10.1006/viro.1993.1180.

50. **Tanabayashi K, Compans RW.** 1996. Functional interactions of paramyxovirus glycoproteins: identification of a domain in Sendai virus HN which promotes cell fusion. J Virol **70:**6112–6118.

51. **Yuasa T, Kawano M, Tabata N, Nishio M, Kusagawa S, Komada H, Matsumura H, Ito Y, Tsurudome M.** 1995. A cell fusion-inhibiting monoclonal antibody binds to the presumed stalk domain of the human parainfluenza type 2 virus hemagglutinin-neuraminidase protein. Virology **206:**1117–1125. http://dx.doi.org/10.1006/viro.1995.1035.

52. **Crennell S, Takimoto T, Portner A, Taylor G.** 2000. Crystal structure of the multifunctional paramyxovirus hemagglutinin-neuraminidase. Nat Struct Biol **7:**1068–1074. http://dx.doi.org/10.1038/81002.

53. **Zaitsev V, von Itzstein M, Groves D, Kiefel M, Takimoto T, Portner A, Taylor G.** 2004. Second sialic acid binding site in Newcastle disease virus hemagglutinin-neuraminidase: implications for fusion. J Virol **78:**3733–3741. http://dx.doi.org/10.1128/JVI.78.7.3733-3741.2004.

54. **Lawrence MC, Borg NA, Streltsov VA, Pilling PA, Epa VC, Varghese JN, McKimm-Breschkin JL, Colman PM.** 2004. Structure of the haemagglutinin-neuraminidase from human parainfluenza virus type III. J Mol Biol **335:**1343–1357. http://dx.doi.org/10.1016/j.jmb.2003.11.032.

55. **Yuan P, Thompson TB, Wurzburg BA, Paterson RG, Lamb RA, Jardetzky TS.** 2005. Structural studies of the parainfluenza virus 5 hemagglutinin-neuraminidase tetramer in complex with its receptor, sialyllactose. Structure **13:**803–815. http://dx.doi.org/10.1016/j.str.2005.02.019.

56. **Bousse T, Takimoto T.** 2006. Mutation at residue 523 creates a second receptor binding site on human parainfluenza virus type 1 hemagglutinin-neuraminidase protein. J Virol **80:**9009–9016. http://dx.doi.org/10.1128/JVI.00969-06.

57. **Ader N, Brindley MA, Avila M, Origgi FC, Langedijk JP, Örvell C, Vandevelde M, Zurbriggen A, Plemper RK, Plattet P.** 2012. Structural rearrangements of the central region of the morbillivirus attachment protein stalk domain trigger F protein refolding for membrane fusion. J Biol Chem **287:**16324–16334. http://dx.doi.org/10.1074/jbc.M112.342493.

58. **Talekar A, DeVito I, Salah Z, Palmer SG, Chattopadhyay A, Rose JK, Xu R, Wilson IA, Moscona A, Porotto M.** 2013. Identification of a region in the stalk domain of the Nipah virus receptor binding protein that is critical for fusion activation. J Virol **87:**10980–10996. http://dx.doi.org/10.1128/JVI.01646-13.

59. **Bose S, Song AS, Jardetzky TS, Lamb RA.** 2014. Fusion activation through attachment protein stalk domains indicates a conserved core mechanism of paramyxovirus entry into cells. J Virol **88:**3925–3941. http://dx.doi.org/10.1128/JVI.03741-13.

60. **Maar D, Harmon B, Chu D, Schulz B, Aguilar HC, Lee B, Negrete OA.** 2012. Cysteines in the stalk of the Nipah virus G glycoprotein are located in a distinct subdomain critical for fusion activation. J Virol **86:**6632–6642. http://dx.doi.org/10.1128/JVI.00076-12.

61. **Bishop KA, Hickey AC, Khetawat D, Patch JR, Bossart KN, Zhu Z, Wang LF, Dimitrov DS, Broder CC.** 2008. Residues in the stalk domain of the Hendra virus G glycoprotein modulate conformational changes associated with receptor binding. J Virol **82:**11398–11409. http://dx.doi.org/10.1128/JVI.02654-07.

62. **Talekar A, Moscona A, Porotto M.** 2013. Measles virus fusion machinery activated by sialic acid binding globular domain. J Virol **87:**13619–13627. http://dx.doi.org/10.1128/JVI.02256-13.

63. **Welch BD, Yuan P, Bose S, Kors CA, Lamb RA, Jardetzky TS.** 2013. Structure of the parainfluenza virus 5 (PIV5) hemagglutinin-neuraminidase (HN) ectodomain. PLoS Pathog **9:**e1003534. http://dx.doi.org/10.1371/journal.ppat.1003534.

64. **Yuan P, Paterson RG, Leser GP, Lamb RA, Jardetzky TS.** 2012. Structure of the Ulster strain Newcastle disease virus hemagglutinin-neuraminidase reveals auto-inhibitory interactions associated with low virulence. PLoS Pathog. **8:**e1002855. http://dx.doi.org/10.1371/journal.ppat.1002855.

65. **Yuan P, Leser GP, Demeler B, Lamb RA, Jardetzky TS.** 2008. Domain architecture and oligomerization properties of the paramyxovirus PIV 5 hemagglutinin-neuraminidase (HN) protein. Virology **378:**282–291. http://dx.doi.org/10.1016/j.virol.2008.05.023.

66. **Paterson RG, Johnson ML, Lamb RA.** 1997. Paramyxovirus fusion (F) protein and hemagglutinin-neuraminidase (HN) protein interactions: intracellular retention of F and HN does not affect transport of the homotypic HN or F protein. Virology **237:**1–9. http://dx.doi.org/10.1006/viro.1997.8759.

67. **Porotto M, Murrell M, Greengard O, Doctor L, Moscona A.** 2005. Influence of the human parainfluenza virus 3 attachment protein's neuraminidase activity on its capacity to activate the fusion protein. J Virol **79:**2383–2392. http://dx.doi.org/10.1128/JVI.79.4.2383-2392.2005.

68. **Markwell MA, Svennerholm L, Paulson JC.** 1981. Specific gangliosides function as host cell receptors for Sendai virus. Proc Natl Acad Sci U S A **78:**5406–5410. http://dx.doi.org/10.1073/pnas.78.9.5406.

69. **Vigant F, Lee J, Hollmann A, Tanner LB, Akyol Ataman Z, Yun T, Shui G, Aguilar HC, Zhang D, Meriwether D, Roman-Sosa G, Robinson LR, Juelich TL, Buczkowski H, Chou S, Castanho MA, Wolf MC, Smith JK, Banyard A, Kielian M, Reddy S, Wenk MR, Selke M, Santos NC, Freiberg AN, Jung ME, Lee B.** 2013. A mechanistic paradigm for broad-spectrum antivirals that target virus-cell fusion. PLoS Pathog **9:**e1003297. http://dx.doi.org/10.1371/journal.ppat.1003297.

70. **Palmer SG, DeVito I, Jenkins SG, Niewiesk S, Porotto M, Moscona A.** 2014. Circulating clinical strains of human parainfluenza virus reveal viral entry requirements for in vivo infection. J Virol **88:**13495–13502. http://dx.doi.org/10.1128/JVI.01965-14.

71. **Suloway C, Shi J, Cheng A, Pulokas J, Carragher B, Potter CS, Zheng SQ, Agard DA, Jensen GJ.** 2009. Fully automated, sequential tilt-series acquisition with Leginon. J Struct Biol **167:**11–18. http://dx.doi.org/10.1016/j.jsb.2009.03.019.

72. **Kremer JR, Mastronarde DN, McIntosh JR.** 1996. Computer visualization of three-dimensional image data using IMOD. J Struct Biol **116:**71–76. http://dx.doi.org/10.1006/jsbi.1996.0013.

73. **Lee KK.** 2010. Architecture of a nascent viral fusion pore. EMBO J **29:**1299–1311. http://dx.doi.org/10.1038/emboj.2010.13.

74. **Pettersen EF, Goddard TD, Huang CC, Couch GS, Greenblatt DM, Meng EC, Ferrin TE.** 2004. UCSF Chimera—a visualization system for exploratory research and analysis. J Comput Chem **25:**1605–1612. http://dx.doi.org/10.1002/jcc.20084.

75. **Fujii T, Iwane AH, Yanagida T, Namba K.** 2010. Direct visualization of secondary structures of F-actin by electron cryomicroscopy. Nature **467:**724–728. http://dx.doi.org/10.1038/nature09372.